

THE GENERATION OF MAGNETIC FIELDS THROUGH DRIVEN TURBULENCE

JUNGYEON CHO¹

Department of Astronomy, University of Texas, Austin, TX 78712; cho@astro.as.utexas.edu

AND

ETHAN T. VISHNIAC

Department of Physics and Astronomy, Johns Hopkins University, Baltimore, MD 21218; ethan@pha.jhu.edu

Received 1999 December 7; accepted 2000 February 24

ABSTRACT

We have tested the ability of driven turbulence to generate magnetic field structure from a weak uniform field using three-dimensional numerical simulations of incompressible turbulence. We used a pseudospectral code with a numerical resolution of up to 144^3 collocation points. We find that the magnetic fields are amplified through field line stretching at a rate proportional to the difference between the velocity and the magnetic field strength times a constant. Equipartition between the kinetic and magnetic energy densities occurs at a scale somewhat smaller than the kinetic energy peak. Above the equipartition scale the velocity structure is, as expected, nearly isotropic. The magnetic field structure at these scales is uncertain, but the field correlation function is very weak. At the equipartition scale the magnetic fields show only a moderate degree of anisotropy, so the typical radius of curvature of field lines is comparable to the typical perpendicular scale for field reversal. In other words, there are few field reversals within eddies at the equipartition scale and no fine-grained series of reversals at smaller scales. At scales below the equipartition scale, both velocity and magnetic structures are anisotropic; the eddies are stretched along the local magnetic field lines, and the magnetic energy dominates the kinetic energy on the same scale by a factor that increases at higher wavenumbers. We do not show a scale-free inertial range, but the power spectra are a function of resolution and/or the imposed viscosity and resistivity. Our results are consistent with the emergence of a scale-free inertial range at higher Reynolds numbers.

Subject headings: ISM: general — MHD — turbulence

1. INTRODUCTION

There are at least two distinct types of magnetohydrodynamic (MHD) turbulence. When the external large-scale magnetic field is strong, the resulting turbulence can be described as the nonlinear interactions of Alfvén waves (e.g., Goldreich & Sridhar 1995; 1997). In contrast, when the external field is weak, MHD turbulence near the scale of the largest energy-containing eddies will be more or less like ordinary hydrodynamic turbulence with a small magnetic back reaction. In this regime, the turbulent eddy turnover time at the large scale (L/V) is less than the Alfvénic time of the scale (L/B), where V and B are rms velocity and magnetic field strength [divided by $(4\pi\rho)^{1/2}$], respectively, and L is the scale of energy injection or the largest energy-containing eddies.

Various aspects of weak/zero external field MHD turbulence have been studied both theoretically and numerically. One of the most important issues in this regime is the generation of large-scale fields. Since large-scale magnetic fields are observed in almost all astrophysical objects, the generation and maintenance of such fields is of great importance. In mean field dynamo theory (see Moffatt 1978; Parker 1979), turbulent motions at small scales are biased to create a nonzero electromotive force along the direction of the large-scale magnetic field. This effect (the “ α -effect”) works to amplify and maintain large-scale magnetic fields. Whether or not this effect actually works depends on the structure of the MHD turbulence, especially on the mobility of the field lines. For example, Vainshtein & Cattaneo

(1992) have argued that when equipartition between magnetic and kinetic energy densities occurs at any scale larger than the dissipation scale, the mobility of the field lines and the α -effect will be greatly reduced. An alternative approach, which may avoid such difficulties, is to appeal to small-scale field line stretching alone to generate strong magnetic fields (Batchelor 1950; Kazantsev 1967). In this model large-scale magnetic fields are actually composed of parallel fibrils of random polarity; i.e., the large-scale field is defined by the preferred axis of the magnetic field direction but there is little large-scale flux in such fields. Whether or not the mean field dynamo mechanism works, it is interesting to contemplate whether or not such fine-grained fields can be produced in the absence of any α -effect.

In addition, there are at least two other points of contention regarding the nature of magnetic fields generated in MHD turbulence. First, the mobility of magnetic fields will be affected by their intermittence. Various models for the generation and dynamics of flux tubes have been proposed, motivated in part by observations of the solar photosphere (e.g., Vishniac 1995a, 1995b; Brandenburg, Proccaccia, & Segel 1995). However, so far numerical simulations have tended to show only modest levels of intermittence. Second, there is the nature of the energy cascade and power spectrum of MHD turbulence. There are numerous analytical models for dealing with MHD turbulence: the eddy-damped quasi-normal Markovian (EDQNM) approximation (Pouquet, Frish, & L  orat 1976), the renormalization group technique (Fournier, Sulem, & Pouquet 1982), and others, including recent work by Goldreich & Sridhar (1995, 1997) in which they treated nonlinear eddy interactions as a series of interactions between marginally nonlinear Alfvén waves. The last is perhaps the most

¹ Department of Physics and Astronomy, Johns Hopkins University, Baltimore, MD 21218.

promising. The energy spectra of MHD turbulence is one of the most poorly understood fields in astrophysics. Early work by Iroshnikov (1963a, 1963b) and Kraichnan (1965) obtained a $k^{-3/2}$ spectrum for both magnetic energy and kinetic energy in the presence of a dynamically significant magnetic field. However, this work was based on the assumption of isotropy in wavenumber space, which is difficult to justify unless the magnetic field is very weak. The model by Goldreich & Sridhar assumes a critical level of anisotropy, such that magnetic and hydrodynamic forces are comparable, and predicts a $k^{-5/3}$ spectrum for strong external field turbulence (which should apply to very small scales within any MHD turbulent cascade). Solar wind observations, which are well within the strongly magnetized regime, show an energy spectrum $E(k) \sim k^{-1.70}$ (Leamon et al. 1998). Numerical studies have only recently been able to address this question. Recent work by Cho & Vishniac (2000) and J. Maron & P. Goldreich (1999, private communication) seems to support the scaling laws of Goldreich & Sridhar.

Here we will concentrate on the structure of magnetic fields in MHD turbulence when the external field is weak. In the case of hydrodynamical turbulence, the energy cascades to smaller scales. If we introduce a weak uniform magnetic field, turbulent motions will stretch the magnetic field lines and divert energy to the small-scale magnetic field. As the magnetic field lines are stretched, the magnetic energy density increases rapidly, until the generation of small-scale magnetic structures is balanced by the magnetic back reaction at some scale between L and the dissipation scale. This will happen when the magnetic and kinetic energy densities associated with a scale l are comparable so that Lorentz forces resist further stretching at or below that scale.² However, stretching at scales larger than l is still possible, and the magnetic energy density will continue to grow if l can increase.³ Eventually, a final stationary state will be reached.

This discussion raises two questions. What is the scale of energy equipartition? What is the magnetic field structure on this scale? The answer to the latter question will depend on the nature of diffusive processes acting on the magnetic field. First, suppose that magnetic field lines are unable to smooth the tangled fields at small scales. Then, as a result of the turbulent energy cascade and the subsequent stretching of magnetic field lines, magnetic fields have thin fibril structures with many polarity reversals within the energy equipartition scale l . Consequently, magnetic structures on the equipartition scale are highly elongated along the local magnetic field direction. This is the kind of picture one obtains by considering passive advection of magnetic fields in a chaotic flow (for a review see Ott 1998). The degree to which this can be applied to a realistic, highly conducting fluid is controversial. On the other hand, if we assume MHD turbulence is always capable of relaxing tangled field lines at small scales, then we expect eddies at the final equipartition scale to be nearly isotropic. That is, the typical radius of curvature of field lines will be comparable to the scale of field reversal. This picture does not imply a clear

expectation for the scale of equipartition in the stationary state. As we will see later, our simulations support the latter picture but with the energy equipartition scale near, but somewhat smaller than, the largest energy-containing eddy scale.

In this paper, we will interpret the results of numerical simulations of MHD turbulence with a weak external field in terms of these models. In § 2, we discuss the numerical method we used and performance of the code. In § 3, we present the results of simulations. Finally, § 4 contains a discussion of the results and our conclusions.

2. NUMERICAL METHOD AND PERFORMANCE OF THE CODE

We used a pseudospectral code to solve the MHD equations in a periodic box of size 2π :

$$\frac{\partial \mathbf{V}}{\partial t} = (\nabla \times \mathbf{V}) \times \mathbf{V} - (\nabla \times \mathbf{B}) \times \mathbf{B} + \nu \nabla^2 \mathbf{V} + \mathbf{f} + \nabla P', \quad (1)$$

$$\frac{\partial \mathbf{B}}{\partial t} = \mathbf{B} \cdot \nabla \mathbf{V} - \mathbf{V} \cdot \nabla \mathbf{B} + \eta \nabla^2 \mathbf{B}, \quad (2)$$

and

$$\nabla \cdot \mathbf{V} = \nabla \cdot \mathbf{B} = 0, \quad (3)$$

where \mathbf{f} is a random forcing term with unit correlation time, $P' \equiv P + \mathbf{V} \cdot \mathbf{V}/2$, \mathbf{V} is the velocity, and \mathbf{B} is the magnetic field divided by $(4\pi\rho)^{1/2}$. Thus, the field \mathbf{B} is, in fact, the Alfvén velocity. The Alfvén velocity of the background field, B_0 , is set to $10^{-3.5}$ in all simulations. Throughout the paper, we consider only cases where viscosity is equal to magnetic diffusivity:

$$\nu = \eta. \quad (4)$$

In the pseudospectral approach, the actual calculations are performed in wavevector space. The nonlinear terms are evaluated in real space using Fourier-transformed variables and their derivatives and then transformed back into their Fourier components. The forcing term consists of 21 Fourier components with $2 \leq k \leq (12)^{1/2}$. The peak of energy injection is at $k \approx 2.5$ ($\equiv k_L$). We adjusted the amplitudes of the forcing components so that $V \approx 1$. We use exactly the same forcing terms for all simulations. Therefore, the external magnetic fields are very weak for all simulations (i.e., $B_0 \ll V$). Each forcing component consists of two parts: a linearly polarized component and a small circularly polarized component with a preferred helicity. The latter was introduced to provide nonzero helicity injection to the turbulence. The resulting fluid helicity is ~ 0.3 – 0.4 for all runs. We use an appropriate projection operator to calculate the $\nabla P'$ term in Fourier space and also to enforce the divergence-free condition ($\nabla \cdot \mathbf{V} = \nabla \cdot \mathbf{B} = 0$). We use up to 144³ collocation points. We use the integration factor technique for kinetic and magnetic dissipation terms and the leapfrog method for the nonlinear terms. At $t = 0$, the magnetic field is uniform and the velocity is in the range $2 \leq k \leq 4$ in wavevector space. We give the parameters for each run in Table 1.

Either physical viscosity (and diffusivity) or hyperviscosity (and hyperdiffusivity) is used in the dissipation terms (see Table 1). The power of hyperviscosity is set to 8,

² The first energy equipartition scale l can be larger than the dissipation scale when the equipartition occurs before the energy cascade reaches the dissipation scale.

³ Our results show that l does increase and the magnetic energy continues to grow.

TABLE 1
RESULTS OF SIMULATIONS

Run	N^3	$\nu = \eta$	B_0^2	V^2	B^2	ϵ	D_M	$T_{v v_2}^a$	$T_{b v_2}^b$	k_e^c	$(t_1, t_2)^d$
REF1.....	96^3	0.0043	10^{-4}	0.773	0.169	0.167	0.088	0.0815	0.0353	...	(500, 560)
REF2.....	64^3	0.015	...	0.85	...	0.163	(300, 750)
REF3.....	96^3	0.0043	...	1.053	...	0.160	(50, 165)
144A.....	144^3	Hyper	10^{-7}	0.649	0.420	0.161	...	0.0519	0.0758	8.4	(60, 240)
128A.....	128^3	0.003	10^{-7}	0.755	0.200	0.166	0.099	0.0794	0.0421	7.1	(100, 210)
96A.....	96^3	0.0043	10^{-7}	0.761	0.170	0.166	0.088	0.0807	0.0364	6.7	(200, 500)
72A.....	72^3	0.0064	10^{-7}	0.792	0.122	0.165	0.070	0.0870	0.0276	6.8	(300, 800)
64A.....	64^3	0.0074	10^{-7}	0.786	0.113	0.166	0.064	0.0835	0.0257	6.6	(300, 800)
64B.....	64^3	0.01	10^{-7}	0.794	0.0804	0.165	0.048	0.0860	0.0019	6.6	(300, 750)
64C.....	64^3	0.015	10^{-7}	0.808	0.0201	0.164	0.013	0.0903	0.0046	8.0	(300, 800)
64D.....	64^3	0.02	10^{-7}	0.774	$< 10^{-4}$	0.164	$\sim 10^{-5}$	(300, 750)

^a $T_{v|v_2} \equiv T_{v|v_k}(k=2)$.

^b $T_{b|v_2} \equiv T_{b|v_k}(k=2)$.

^c Equipartition wavelength.

^d Time interval used for averaging physical quantities.

such that the dissipation term in the above equation is replaced with

$$-v_8(\nabla^2)^8 V, \quad (5)$$

where v_8 is determined from the condition $v_h(N/2)^{2h}\Delta t \approx 0.5$ (see Borue & Orszag 1995, 1996). Here Δt is the time step and N is the number of grids in each direction. The same expression is used for the magnetic dissipation term.

When $f = \nu = \eta = 0$, that is, without forcing or dissipation, the total energy drops by 0.87% after 13 time units, apparently as a result of truncation errors. In the dissipative case the injection and dissipation of energy are well balanced after the magnetic energy reaches the stationary state:

$$\langle \epsilon \rangle = \langle D_K \rangle + \langle D_M \rangle, \quad (6)$$

where ϵ is the energy injection rate and D_K and D_M are the kinetic and the magnetic energy dissipation rates, respectively. The angle brackets stand for an appropriate space-time average, which is taken after the magnetic energy reaches the stationary state.

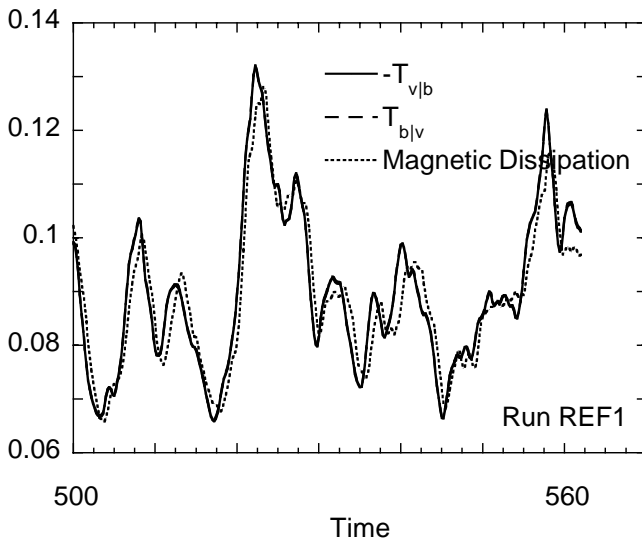


FIG. 1.—Test of the code. Time evolution of $T_{b|v}$, $T_{v|b}$, and magnetic dissipation. $T_{b|v}$ and $-T_{v|b}$ coincide exactly. Magnetic dissipation shows a time delay, which is the turbulent diffusion timescale. Run REF1.

Before we describe the third test, we define several transfer functions. Imagine velocity components in a thin (i.e., thickness = 1) spherical shell of radius k in Fourier space. The work done to the velocity components by magnetic fields can be written as follows:

$$- \sum_{k \leq |\mathbf{p}| < k+1} \hat{V}(\mathbf{p})^* \cdot [(\nabla \times \hat{\mathbf{B}}) \times \mathbf{B}](\mathbf{p}), \quad (7)$$

where carets indicate Fourier space variables and the asterisk denotes a complex conjugate. This relation is derived from the second term on the right-hand side of equation (1). This quantity is the *negative* of the energy transferred to the magnetic fields from the velocity components per unit time:

$$T_{b|v_k}(k) = + \sum_{k \leq |\mathbf{p}| < k+1} \hat{V}(\mathbf{p})^* \cdot [(\nabla \times \hat{\mathbf{B}}) \times \mathbf{B}](\mathbf{p}). \quad (8)$$

Note that the subscripts of $T_{X|Y}$ read “to X from Y .” Similarly, from the first term on the right-hand side of equation (1), we obtain $T_{v|v_k}(k)$:

$$T_{v|v_k}(k) = - \sum_{k \leq |\mathbf{p}| < k+1} \hat{V}(\mathbf{p})^* \cdot [(\nabla \times \hat{\mathbf{V}}) \times \mathbf{V}](\mathbf{p}). \quad (9)$$

Now, consider the magnetic components in the same shell. From the first term on the right-hand side of equation (2), we obtain the energy transferred to the velocity fields from the magnetic components per unit time:

$$T_{v|b_k}(k) = - \sum_{k \leq |\mathbf{p}| < k+1} \hat{\mathbf{B}}(\mathbf{p})^* \cdot (\mathbf{B} \cdot \nabla \mathbf{V})(\mathbf{p}), \quad (10)$$

the work done to the magnetic components by velocity fields: again, this quantity is the *negative* of the work done to the magnetic components by velocity fields per unit time.

In our third test, we checked the energy budget of the magnetic fields. The *net* energy transferred to magnetic fields from velocity fields can be calculated from either $T_{b|v_k}(k)$ or $T_{v|b_k}(k)$. This energy will disappear through diffusive damping. Therefore, the numerical scheme should satisfy

$$T_{b|v} = -T_{v|b} = D_M, \quad (11)$$

where

$$T_{b|v} \equiv \sum_{k=0}^{k_{\max}} T_{b|v_k}(k), \quad (12)$$

$$T_{v|b} \equiv \sum_{k=0}^{k_{\max}} T_{v|b_k}(k), \quad (13)$$

and k_{\max} is the largest wavenumber in Fourier space and is equal to $N/2$. Figure 1 shows that our code satisfies equation (11). The two curves $T_{b|v}(t)$ and $-T_{v|b}(t)$ coincide exactly. It is interesting to note that there is a time delay between $T_{b|v}$ ($=T_{v|b}$) and D_M , which is a measure of the energy cascade time.

3. RESULTS

3.1. Generation of Magnetic Fields

We list the results of our simulations in Table 1. We obtained V^2 , B^2 , ϵ , and D_M by averaging over (t_1, t_2) using all available data. However, $T_{v|v_2}$ [$\equiv T_{v|v_k}(k=2)$] and $T_{b|v_2}$ [$\equiv T_{b|v_k}(k=2)$] were calculated from a sparse subset of the data. It is important to note that, unless otherwise noted, these time averages were taken after the turbulence had reached the stationary state. Conclusions based on these averages do not apply to the initial growth phase of the magnetic field.

Figure 2 shows time evolution of kinetic and magnetic energy density. All the simulations have similar kinetic energy densities. However, the magnetic energy density obviously depends on the ohmic diffusivity η . After an initial growth phase, the magnetic energy reaches a stationary state. The initial growth rate of the magnetic energy depends on diffusivity. Even though it is not clearly shown in the figure, the initial growth phase consists of two stages for run 144A, the hyperviscosity run. In the first stage, which begins at $t=0$ and ends after a few dynamical times, the growth rate is very fast. At this stage the magnetic energy grows through the stretching of magnetic field lines. Growth is fast because there is no significant back reaction by the magnetic fields. Figure 3 shows that stretching is initially most active near or somewhat larger than the dissipation scale (cutoff scale) and the magnetic energy spectrum peaks at this scale. As the magnetic energy grows, the magnetic back reaction becomes important at the dissipation

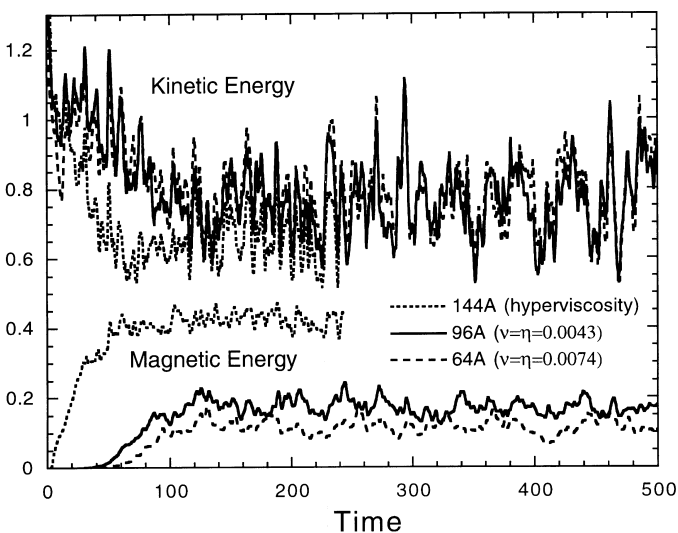


FIG. 2.—Time evolution of kinetic and magnetic energy. The results at three different resolutions are shown: 144^3 (run 144A; dotted curve), 96^3 (run 96A; solid curve), and 64^3 (run 64A; dashed curve). For 64A and 96A, the kinetic energy has very similar values. The magnetic energy depends on ν ($=\eta$). In the case of hyperviscosity (run 144A), the magnetic energy is more than one-half of the kinetic energy.

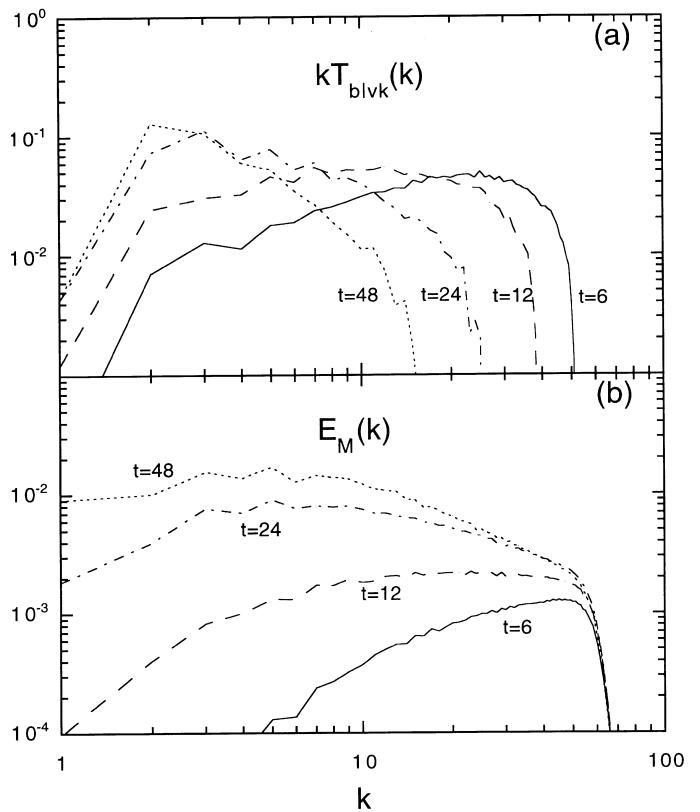


FIG. 3.—Time evolution of $kT_{b|v_k}(k)$ and $E_M(k)$. Run 144A.

scale. When energy equipartition is reached at this scale, the stretching rate slows down and a second stage of slower growth begins. Figure 3 shows that during this stage the peak of the magnetic power spectrum moves to larger scales. Figure 2 shows that the second stage ends at $t=30 \sim 40$ for run 144A. Other runs with physical viscosities (run 128A, 96A, 64A, etc.) also show similar behavior. However, the detailed evolution seems different from the hyperviscosity case. For example, the diffusivity also affects the net growth rate in the second stage.

In Figure 4a, we plot the kinetic and magnetic energy densities as functions of ν ($=\eta$). Error bars are estimated from

$$2 \frac{\langle X^2 \rangle - \langle X \rangle^2}{\sqrt{(t_2 - t_1)/t_{\text{corr}}}}, \quad (14)$$

where angle brackets denote the time average and $X = V$ and B . As noted above, this average is taken after the turbulence has reached its stationary state. The correlation time $t_{\text{corr}} \sim 3$ is calculated directly. We see that the kinetic energy is almost independent of ν ($=\eta$). The constancy of the kinetic energy density is the result of the magnetic field. In purely hydrodynamic simulations the kinetic energy density increases as ν decreases (see REF2 and REF3 in Table 1). On the other hand, the magnetic energy increases as ν ($=\eta$) decreases. This figure suggests that at small η even a weak diffuse magnetic field can lead to a strong final state. In the case of hyperviscosity, the magnetic energy is almost one-half of the kinetic energy at late times. This is the result of field line stretching and not the α -effect (see next paragraph and § 4). The energy injection rates ϵ ($\equiv f \cdot V = D_K + D_M$) are independent of ν ($=\eta$) and in the range $0.161 < \epsilon < 0.166$ (Table 1).

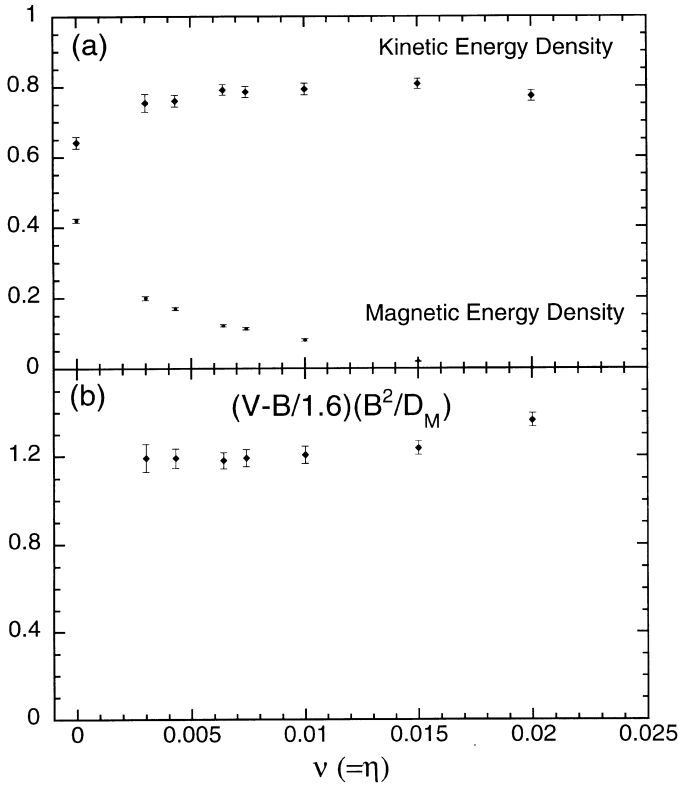


FIG. 4.—Dependence of physical quantities on $\nu (= \eta)$. *Top*: The kinetic energy density is nearly independent of the physical viscosity. The magnetic energy density grows as $\nu (= \eta)$ decreases. *Bottom*: This relation implies $D_M \sim (V - B/1.6)B^2$.

In Figure 4b, we plot an empirical relation for the generation of magnetic fields in the stationary state:

$$D_M \sim \left(\frac{V}{L} - c \frac{B}{L} \right) B^2, \quad (15)$$

where c is a constant (~ 0.63). It is somewhat dangerous to assume that run 144A, the hyperviscosity run, is equivalent to the case of vanishing viscosity. In particular, Figure 5 shows a sharp rise in the energy transfer to the magnetic field near the dissipation scale. This makes it difficult to extend this relationship to the case of vanishing diffusivity.⁴

What is the origin of this correlation? In the stationary state, the magnetic dissipation (D_M) is balanced by the net energy transferred to the magnetic fields from the velocity fields. The right-hand side therefore tells us that the net energy transferred to the magnetic fields is proportional to the large-scale eddy turnover rate (V/L) minus an Alfvénic

⁴ In run 144A, the magnetic dissipation is given by $\sum v_8 k^{16} |\hat{B}|^2$. Although we can calculate this quantity directly, we should not use this for eq. (15) because D_M in eq. (15) actually represents the amount of energy transferred to the magnetic field on large scales. If we use a physical viscosity (and diffusivity), the two quantities are the same. However, in hyperviscosity runs, the two quantities diverge because nonlinear processes occurring near the dissipation cutoff are presumably unphysical. The dotted curve in Fig. 5 represents the amount of energy transferred to the magnetic field in run 144A. The curve shows a nonnegligible change after the dissipation cutoff ($k_d \sim 50$), which means that nonlinear processes do occur within the dissipation range (i.e., $k > k_d$). If we take the value of $\Pi_{b|v_k}$ at $k \sim k_d$ for D_M and substitute it into eq. (15), then we obtain $(v - B/1.6)B^2/D_M = 1.24$, in good agreement with the other data shown in Fig. 4b. This suggests that eq. (15) is true even in the limit of vanishing viscosity (and diffusivity), but given the existence of anomalous energy transfer near the dissipation scale, this conclusion may be premature.

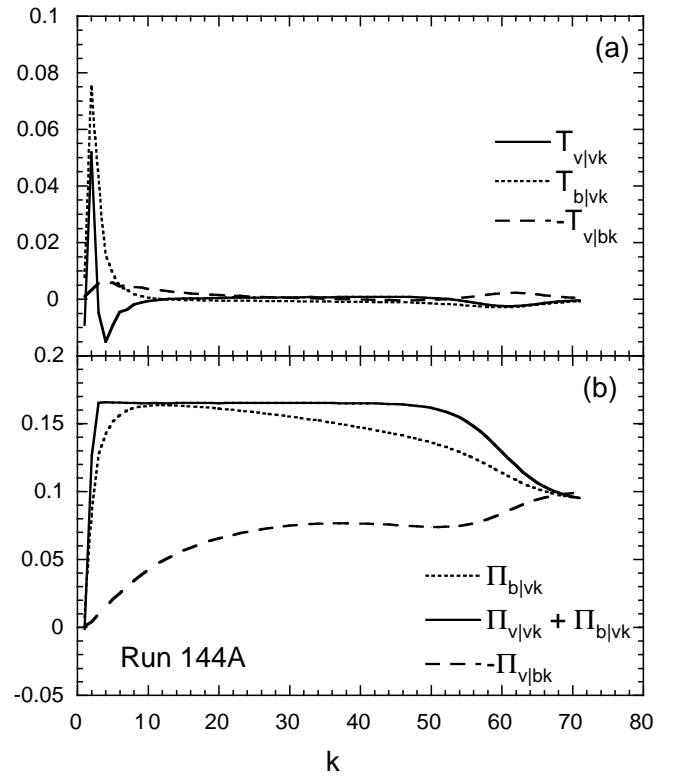


FIG. 5.—Energy transfer and flux spectra for run 144A. *Top*: Energy transfer spectra. The spectrum of $T_{b|v_k}$ (dotted curve) shows that magnetic fields gain energy from large-scale eddies. *Bottom*: Energy flux spectra. The spectrum of $\Pi_{b|v_k}$ (dotted curve) rises rapidly at small k and reaches the value of ϵ at $k \sim 10$.

frequency (B/L) times a constant. The large-scale eddy turnover rate is equal to the stretching rate of the magnetic field when the back reaction is zero. We identify the second term on the right-hand side of this equation as the effect of the magnetic back reaction.

This interpretation is supported by the spectrum of the energy transfer rate, $T_{b|v_k}(k)$. The function $T_{b|v_k}(k)$ is the energy lost by velocity components within a unit shell of radius k in wavevector space through interactions with the magnetic field. When this quantity is positive, it means that energy is being transferred from velocity components in the unit shell to the magnetic field. In Figure 5a, we plot $T_{v|v_k}(k)$, $T_{b|v_k}(k)$, and $T_{v|b_k}(k)$ for run 144A. From the spectrum of $T_{b|v_k}(k)$ we can see that magnetic fields are driven by energy extracted from the large-scale velocity components (cf. Kida, Yanase, & Mizushima 1991). We can explain this result if we suppose that the magnetic field energy is generated by field line stretching at large scales. On the other hand, the magnetic fields have a small rate of net energy transfer to small-scale motions, implying that on small scales the turbulent motions can be described as nonlinear Alfvén waves, with a rough balance between kinetic and magnetic energy densities.

In Figure 5b, we plot the spectra of energy fluxes. The energy flux $\Pi_{b|v_k}(k)$ is the amount of energy transferred from velocity components whose wavenumbers are less than or equal to k , to the magnetic components of all wavenumbers:

$$\Pi_{b|v_k}(k) = \int_0^k T_{b|v_p}(p) dp. \quad (16)$$

We define other fluxes similarly. The graph of $\Pi_{b|v_k}(k)$ rises rapidly at large scales ($k < 10$) and reaches the value of energy injection rate ϵ (~ 0.16) at $k \sim 10$. This means that the energy injected to drive the turbulence (~ 0.16 per unit time) is absorbed at large scales by the magnetic fields. On smaller scales ($k > 10$) the velocity field does not drive the magnetic fields but instead *absorbs* energy. In summary, the rise of $\Pi_{b|v_k}(k)$ at small wavenumbers is due to field line stretching, and the decrease at large wavenumbers is a sign of Alfvénic turbulence at small scales. Consequently, at small scales, we can treat the turbulent motions as fully developed MHD turbulence, even when external fields are weak.

Before proceeding, it is useful to take note of a property of hyperviscosity simulations. The quantity $\Pi_{v|v_k}(k) + \Pi_{b|v_k}(k)$ is the total energy transferred from large-scale velocity fields ($|k| < k$) to either magnetic fields or small-scale velocity fields. When there is no dissipation, the energy injected by the driving force is either transferred to magnetic fields or transferred to small-scale velocity fields:

$$\epsilon = \Pi_{v|v_k}(k) + \Pi_{b|v_k}(k). \quad (17)$$

That is, the quantity $\Pi_{v|v_k}(k) + \Pi_{b|v_k}(k)$ has to be a constant for a hyperviscosity simulation. In fact, in the hyperviscosity simulation (run 144A), this quantity is constant for $k < 50$.

In Figure 6, we plot $T_{v|v_2}$ and $T_{b|v_2}$. Here $T_{v|v_2}$ [$\equiv T_{v|v_k}(k=2)$] is proportional to the rate at which the energy of large-scale eddies is transferred to small-scale velocity fields. On the other hand, $T_{b|v_2}$ [$\equiv T_{b|v_k}(k=2)$] is proportional to the rate at which the energy of large-scale eddies is transferred to magnetic fields. Note that $k=2$ corresponds to the scale of the largest energy-containing eddies. Figure 6a shows

$$T_{v|v_2} \sim V^3, \quad (18)$$

which suggests that large-scale kinetic energy (V^2) is transferred to smaller scales within an eddy turnover time (L/V). That is, turbulence at large scale is broadly similar to ordinary hydrodynamic turbulence and the classical energy cascade model seems to work. In the case of hyperviscosity, the figure suggests that the energy transfer rate may not exactly follow the scaling relation given above. However, as we can see in the figure, the deviation, if any, will be very small.

Figure 6b shows

$$T_{b|v_2} \sim B^2 V. \quad (19)$$

When a magnetic field is generated through the stretching of field lines, $T_{b|v_2}$ will be proportional to the stretching rate at large scales. Although equation (15) implies that the overall stretching rate is proportional to $(V - \text{const} \times B)$, Figure 6b suggests that the stretching rate scales as $B^2 V$ at the largest energy-containing eddy scale. That is, it is proportional to the large eddy turnover rate V/L .

3.2. The Structure of Turbulence

We plot energy spectra in Figure 7. For all simulations using physical viscosities (runs 128A, 96A, 72A, and 64A–D) the kinetic energy spectra are almost independent of ν at large scales ($k < 10$). However, this is not true in the case of hyperviscosity (run 144A). Magnetic energy spectra peak near but somewhat smaller than the energy injection scale. The position of the peaks depends on magnetic diffusivity.

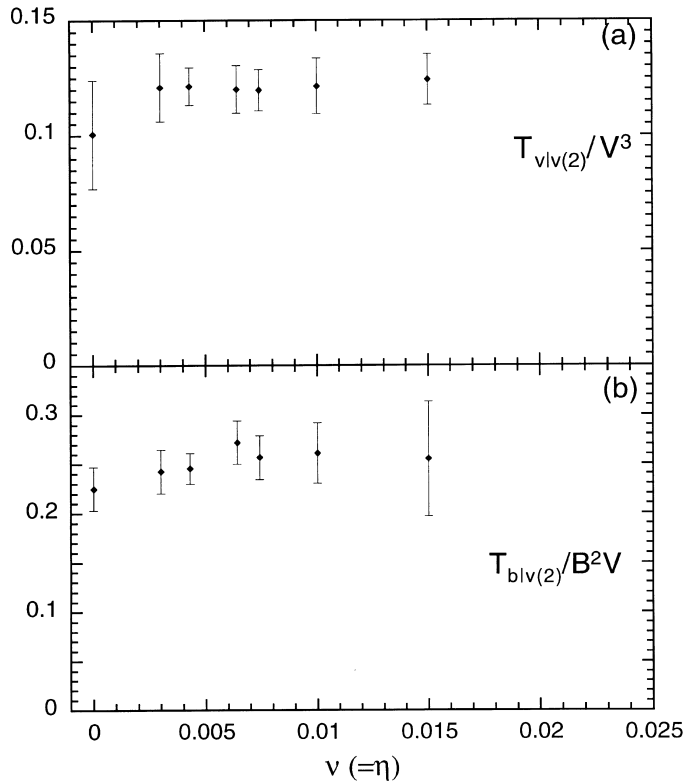


FIG. 6.—Evidence that large-scale turbulence is similar to ordinary hydrodynamic turbulence. *Top*: $T_{v|v_k}(k=2)/V^3$ is nearly constant for nonzero physical viscosity, which implies that $T_{v|v_k}(k=2) \sim V^3$. In the case of hyperviscosity, this relation may not hold true. *Bottom*: $T_{b|v_k}(k=2)/(B^2V)$. This relation implies stretching of magnetic field lines without significant back reaction is responsible for the nonlinear energy transfer from velocity components at $k \sim 2$ to magnetic fields.

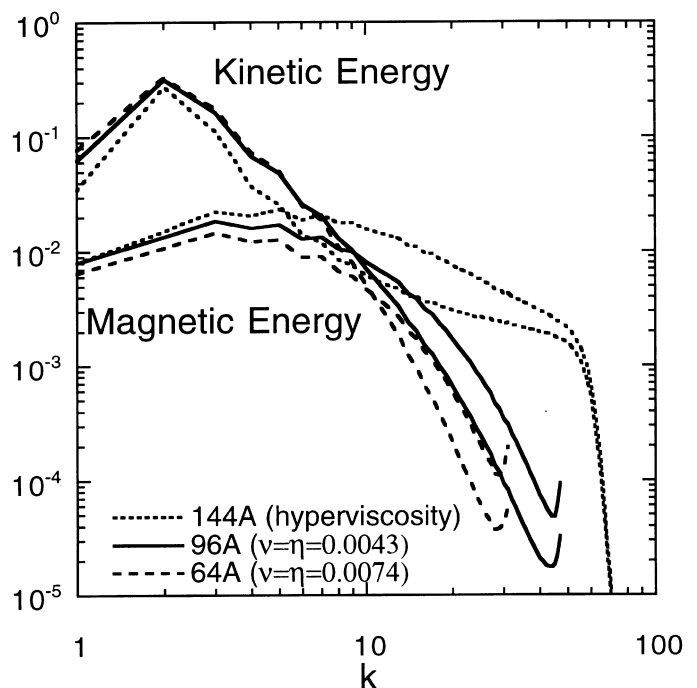


FIG. 7.—Energy spectra. The results at three different resolutions are shown: 144^3 (run 144A; dotted curve), 96^3 (run 96A; solid curve), and 64^3 (run 64A; dashed curve). Both axes are drawn on a logarithmic scale.

We see that the location of the peaks moves toward the largest scale as diffusivity increases. In the case of the hyperviscosity (and hyperdiffusivity) simulation, both kinetic and magnetic spectra show the well-known bottleneck effect (see, e.g., Borue & Orszag 1996) for $k > \sim 20$. This effect is characterized by a local enhancement of the energy spectra at scales somewhat larger than the dissipation cutoff.

We define the energy equipartition wavenumber k_e , such that

$$\int_0^{k_e} dp E_M(p) = \int_{k_e}^{k_{\max}} dp E_K(p). \quad (20)$$

In this definition, energy equipartition between *large*-scale magnetic fields and *small*-scale velocity fields occurs at $k = k_e$. [Therefore, k_e is different from the scale of equipartition between *small*-scale magnetic energy and *small*-scale kinetic energy. A good measure for the equipartition scale between small-scale energies is the wavenumber at which $E_K(k) = E_M(k)$. In the case of hyperviscosity, the two wavelengths are similar.] From Table 1, we can see that k_e is not very sensitive to the value of viscosity. In all cases, the equipartition scale ($\sim 1/k_e$) is somewhat smaller than the peak of the kinetic energy spectrum ($1/k_L \sim 1/2.5$). The magnetic fields associated wavenumbers greater than k_e act like a strong uniform external magnetic field for eddies smaller than $\sim 1/k_e$, and the structure of turbulence at smaller scales will be similar to Alfvénic turbulence. On the contrary, turbulence at scales larger than $\sim 1/k_e$ will be more or less like ordinary hydrodynamic turbulence. This argument is supported by the fact that the value of k_e is very close to the peak of $\Pi_{b|v_k}(k)$ for all runs. For example, Figure 5b shows that $\Pi_{b|v_k}(k)$ peaks at $k \sim 10$ for run 144A. Table 1 shows that $k_e \sim 8.4$ for the same run. [Our analysis also shows that, for run 96A, $k_e \sim 6.7$ and $\Pi_{b|v_k}(k)$ peaks at $k \sim 8$. In addition, for run 64A, $k_e \sim 6.6$ and $\Pi_{b|v_k}(k)$ peaks at $k \sim 8$...] This suggests that, below the equipartition scale, the turbulent fluid is in a state of nonlinear Alfvénic turbulence, with a fixed ratio between the kinetic and magnetic energies associated with perturbations on these scales.

We see that a small external field leads to local magnetic energy density, which, in the limit of very small diffusivity, is comparable to the kinetic energy density, with a typical scale only slightly smaller than the scale at which the turbulence is driven. This still leaves the question of whether the magnetic field is characterized by numerous polarity reversals within each eddy. We have examined this question by considering the magnetic field second-order structure function. A detailed description of our method can be found in Cho & Vishniac (2000). Here we note only that we define the structure function in cylindrical coordinates as

$$F(\rho, z) = \langle |Y(\mathbf{r}_1) - Y(\mathbf{r}_2)|^2 \rangle, \quad (21)$$

where Y can be either the magnetic field or the velocity. The coordinates are defined relative to the *local* field direction, with ρ being the distance perpendicular to $[\mathbf{B}(\mathbf{r}_1) + \mathbf{B}(\mathbf{r}_2)]/2$ and z the distance parallel to it.

We plot the results for run 144A in Figure 8. The shape of the contours represents the average shape of the eddies, which in turn reflects the degree of anisotropy along the local field direction. As expected, the velocity field shows isotropy at large scales and anisotropy at small scales. The magnetic fields show an insignificant amount of correlation at large scales and strong anisotropy at small scales. At

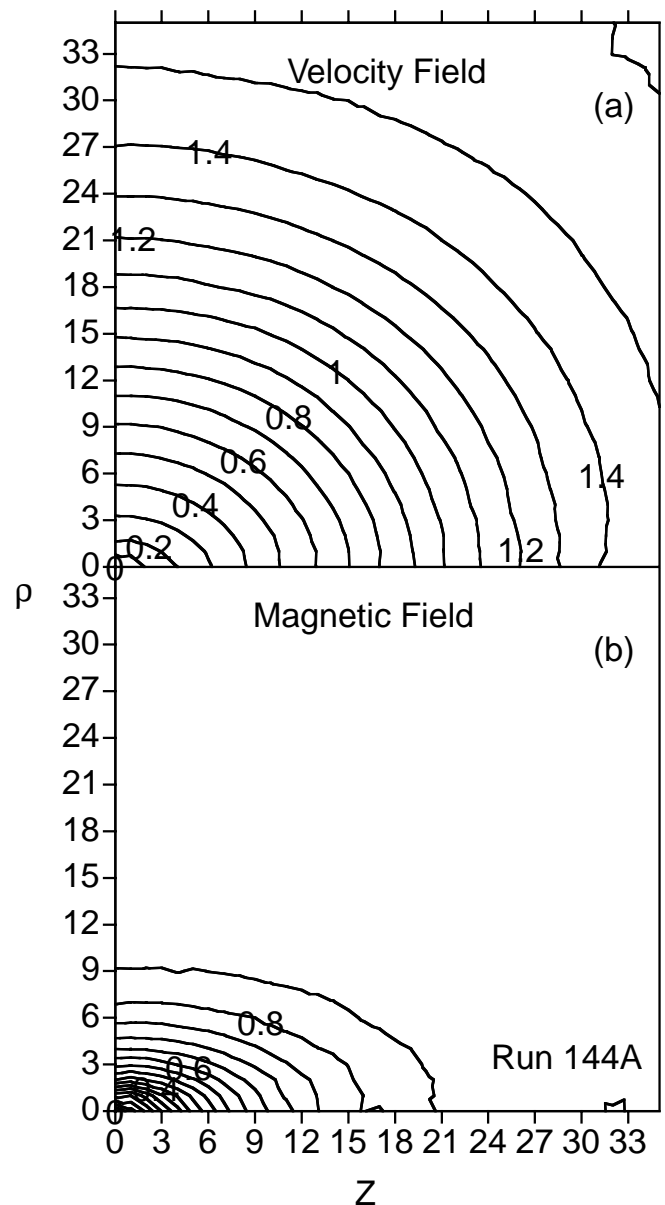


FIG. 8.—Second-order structure functions for the magnetic and velocity fields. The horizontal axis is in the direction of the local magnetic field, defined by pairwise averaging. The velocity fields show correlations at all scales, with a smooth transition from isotropy on large scales to anisotropy on small scales. The magnetic field shows similar behavior on small scales, below the equipartition scale, but has almost no correlation on large scales.

intermediate scales, comparable to the equipartition scale, the magnetic field shows a factor of 2 difference in correlation lengths along local field line directions and across them. The implication is that the field is *not* composed of numerous parallel fibrils with frequent polarity reversals on small scales, as envisioned by Batchelor (1950) and Kazantsev (1967). Instead, the field is largely smoothed by small-scale turbulent diffusion and shows only one or two polarity reversals at its typical scale of organization.

4. DISCUSSION AND CONCLUSIONS

We have presented results of MHD numerical simulations for unit magnetic Prandtl number (i.e., $\nu = \eta$). A weak diffuse magnetic field was used as an initial condition, and we tested the sensitivity of our results to dissipative effects

by varying the viscosity and numerical resolution in our simulations. We have found that magnetic fields are amplified through field line stretching at a rate proportional to $(V - cB)/L$, where $c \sim 0.63$. It is not certain whether or not the hyperviscosity run follows this relation. We have also shown that, in the limit of $\nu (= \eta) \rightarrow 0$, the magnetic field reaches a final stationary state where the magnetic energy density is comparable to the kinetic energy. Since the simulations using physically realistic functional forms for the diffusivity are very far away from this limit, we are not able to extrapolate to a definite final ratio of E_B/E_K , but it should be at least as large as the value reached in run 144A, ~ 0.6 . The typical scale of the magnetic field is slightly smaller than the scale of the largest energy-containing eddies. At or above the equipartition scale, eddies are almost isotropic. However, eddies smaller than the equipartition scale show elongation along the local magnetic field lines.

When we vary viscosity (and diffusivity) explicitly, physical quantities scale as follows:

1. $V^2 \sim \text{const}$,
2. $D_M \sim (V - cB)B^2$, $c = \text{const}$,
3. $T_{v|v_k}(k=2) \sim V^3$, and
4. $T_{b|v_k}(k=2) \sim VB^2$.

The turbulent dynamo effect did not play a role in these simulations. There is no sign of the spontaneous generation of a large-scale field, above what we would expect by extrapolating the magnetic energy power spectrum to wavenumbers smaller than the energy peak. Our results are most plausibly explained in terms of random field line stretching within eddies. We have tested this conclusion by conducting additional simulations with no imposed helicity. The results were almost identical to the simulations presented here. However, this does not allow us to draw any general conclusions about the possibility of mean field dynamos in astrophysical objects. We note that the average helicity for all the runs listed in Table 1 is in the range 0.3–0.4. Since the smallest allowable wavenumber is 1, this implies a maximum mean field growth rate of order 0.1 times the eddy correlation time. By comparison, the turbulent dissipation rate is $\langle V^2 \rangle / 3$ (or ~ 0.3) times the eddy correlation time. The obvious conclusion is that no dynamo effect is expected. The energy injection scale here is too close to the size of the computational box.

The isotropic structure of eddies at large scales in our simulations implies something about diffusive processes in MHD turbulence. In particular, it suggests the presence of an effective magnetic diffusivity, which is tied to the large-scale eddy size rather than the resistive scale. This is an old idea (see, e.g., Parker 1955) and is equivalent to the notion that the usual turbulent diffusion coefficients can be substituted for ohmic resistivity. In its original form it was based on a picture of small-scale field line mixing, which has been convincingly criticized by Parker (1992). However, it can also be justified by appealing to rapid reconnection, that is, field line reconnection at rates that are comparable to an eddy turnover rate and much more rapid than estimates based on the Sweet-Parker reconnection rate (Sweet 1958; Parker 1957). In terms of our simulations, we note that if reconnection is slow then we expect that magnetic fields will show a thin fibril structure in the saturated state, with a typical field reversal scale much smaller than the curvature scale. We see from the structure function that this is not the

case. Apparently, in our simulations at least, reconnection is fast enough to relax tangled magnetic field structures in no more than an eddy turnover time. Either the suppression of reconnection appears suddenly at higher resolutions, or theoretical arguments suggesting fast reconnection in highly conducting turbulent fluids (Lazarian & Vishniac 1999) are correct. If the latter interpretation holds up, then arguments suggesting the suppression of the α -effect (e.g., Vainshtein & Cattaneo 1992) at high Reynolds numbers are unlikely to prove correct.

In what follows, we will give a rough explanation for the dependence of field quantities on $\nu (= \eta)$. Readers are advised that this analysis might fail in the limit of vanishing diffusivity. The reason is that run 144A shows slight deviations from the extrapolation results (see V^2 in Fig. 4a and $T_{b|v_2}$ in Fig. 6a). However, in most cases, the deviation is small.

The kinetic energy depends on both viscosity and magnetic energy. The result shown in Figure 4a, that the kinetic energy is almost independent of $\nu = \eta$, is actually the result of a rough cancellation between these two competing effects. Suppose that magnetic field is turned off and, therefore, the turbulence is ordinary hydrodynamic turbulence. Let us also suppose that the viscosity is zero. Then, at the energy injection scale, we will have

$$V^3 \sim \epsilon. \quad (22)$$

This is a well-known relation in Kolmogorov phenomenology wherein the energy injection rate ϵ is equal to the energy cascade rate at the largest energy-containing scale, which is proportional to the energy contained in the largest eddies ($\sim V^2$) divided by 1 eddy turnover time ($\sim L/V$). When viscosity is not extremely small, we need to add a viscosity effect:

$$V^3 + \nu V^2 \sim \epsilon, \quad (23)$$

where we omit constants of order unity in each term. The second term on the left-hand side is proportional to dissipation at the large scale. Since the second term on the left-hand side is much smaller than the first, we can assume that $\nu V^2 \propto \nu + O(\nu^2)$. If we solve this relation for V^2 , we obtain

$$V^2 \sim C_\epsilon \epsilon^{2/3} - C_\nu \nu, \quad (24)$$

where C_ϵ and C_ν are constants. Now if we turn on the magnetic fields and set the viscosity to be zero, then we have

$$V^3 + B^2 V \sim \epsilon. \quad (25)$$

Here we also omit constants of order unity in each term. The first term on the left-hand side is still proportional to V^3 , which is supported by the relation $T_{v|v_2} \propto V^3$ (Fig. 6a). The second term on the left-hand side comes from the relation $T_{b|v_2} \propto VB^2$ (Fig. 6b). Since the second term is small compared with the first, we can write $B^2 V \propto B^2 + O(B^4)$. Solving for V^2 , we have

$$V^2 \sim C_\epsilon \epsilon^{2/3} - C_B B^2. \quad (26)$$

If we combine the two relations, we have

$$V^2 \sim C_\epsilon \epsilon^{2/3} - C_\nu \nu - C_B B^2, \quad (27)$$

where we ignore the interactions between the ν effect and the B^2 effect. If any, such interactions will be weak because both the ν effect and the B^2 effect are weak. This equation implies that the quantity $V^2 + C_B B^2$ depends only on ν .

To complete the above analysis, we need an expression for B^2 . To this end, let us adopt an energy cascade model analogous to the ordinary hydrodynamical case: the energy *transfer* rate is equal to the *magnetic* energy cascade rate at the large scale. The energy transfer rate is given in equation (15). The magnetic energy cascade rate is $B^2/(L/V)$. Therefore, we have

$$(V - B)B^2 \sim B^2V + \eta B^2, \quad (28)$$

where the second term on the right-hand side is the large-scale dissipation term. Again, we omit all order unity constants. If we solve the equation for B , we obtain

$$B = C_V V - C_\eta \eta, \quad (29)$$

where C_V and C_η are constants. In fact, our calculation shows that

$$\frac{B - 0.6V}{\eta} = -26.7 \pm 2.1 \quad (30)$$

for runs 128A, 96A, 72A, 64A, 64B, 64C, and 64D. It implies that $C_V = 0.6$ and $C_\eta \sim 26$. This relation slightly underestimates the magnetic field strength for run 144A. (It gives $B \sim 0.6V$, as opposed to the observed value of $0.8V$.) If we examine Figure 7 we see that this discrepancy arises from the difference between the rms magnetic field strength and the magnetic field strength on the largest eddy scale. Comparing the hyperviscosity run (144A) with the other cases we see that the former has a substantially greater fraction of its magnetic energy in small-scale structures. If we interpret B in the preceding equation as the average obtained by smoothing on the large eddy scale, which is consistent with our derivation, then the hyperviscosity run is in agreement with equation (30). In this sense, the values of B and B^2

present in this discussion section should be regarded as lower limits for the case of vanishing diffusivity. Alternatively, one might regard the following discussion as valid for cases of moderate magnetic Reynolds numbers and that this analysis sets limits for the case of zero diffusivity. For B^2 , we have

$$B^2 \sim C_V^2 V^2 - 2C_V C_\eta V \eta. \quad (31)$$

Here we omitted $C_\eta^2 \eta^2$ on the right-hand side.

If we combine expressions for V^2 and B^2 , we have

$$V^2 \sim (C_\epsilon \epsilon^{2/3} - C_V v + C_\eta \eta)/(1 + C_B C_V^2), \quad (32)$$

$$B^2 \sim (C_V^2 C_\epsilon \epsilon^{2/3} - C_V^2 C_V v - C_V C_\eta V \eta)/(1 + C_B C_V^2). \quad (33)$$

Note that, even though we treat v and η separately, there is no guarantee that the above relations are true for nonunity Prandtl numbers. Since $v = \eta$ and the second and third terms on the right-hand side of equation (32) have different signs, V^2 depends on $v (= \eta)$ weakly. We expect C_B and C_V to have similar values because they are describing similar things: dissipation. The expression for B^2 is not absolutely correct because the omitted term in equation (31) becomes nonnegligible when η becomes large.

When $v = \eta = 0$, we have

$$V^2 \sim C_\epsilon \epsilon^{2/3}/(1 + C_B C_V^2), \quad (34)$$

$$B^2 \sim C_V^2 C_\epsilon \epsilon^{2/3}/(1 + C_B C_V^2). \quad (35)$$

These give a lower limit for B^2 and an upper limit for V^2 .

This work was partially supported by the National Computational Science Alliance under CTS980010N and utilized the NCSA SGI/Cray Origin 2000.

REFERENCES

- Batchelor, G. 1950, Proc. R. Soc. London A, 201, 405
 Borue, V., & Orszag, S. A. 1995, Europhys. Lett., 29(9), 687
 ———. 1996, J. Fluid Mech., 306, 293
 Brandenburg, A., Procaccia, I., & Segel, D. 1995, Phys. Plasmas, 2(4), 1148
 Cho, J., & Vishniac, E. T. 2000, ApJ, in press
 Fournier, J., Sulem, P., & Pouquet, A. 1982, J. Phys. A, 15, 1393
 Goldreich, P., & Sridhar, H. 1995, ApJ, 438, 763
 ———. 1997, ApJ, 485, 680
 Iroshnikov, P. 1963a, AZh, 40, 742
 ———. 1963b, Astron. Zh., 40, 742 (Soviet Astron., 7, 566)
 Kazantsev, A. P. 1967, J. Exp. Theor. Phys., 53, 1806
 Kida, S., Yanase, S., & Mizushima, J. 1991, Phys. Fluids A, 3(3), 457
 Kraichnan, R. 1965, Phys. Fluids, 8, 1385
 Lazarian, A., & Vishniac, E. T. 1999, ApJ, 517, 700
 Leamon, R. J., Smith, C. W., Ness, N. F., Matthaeus, W. H., & Wong, H. K. 1998, J. Geophys. Res., 103, 4775
 Moffatt, H. K. 1978, Magnetic Field Generation in Electrically Conducting Fluids (Cambridge: Cambridge Univ. Press)
 Ott, E. 1998, Phys. Plasmas, 5(5), 1636
 Parker, E. N. 1955, ApJ, 122, 243
 ———. 1957, J. Geophys. Res., 62, 509
 ———. 1979, Cosmical Magnetic Fields (Oxford: Oxford Univ. Press)
 ———. 1992, ApJ, 401, 137
 Pouquet, A., Frish, U., & Léorat, J. 1976, J. Fluid Mech., 77, 321
 Sweet, P. A. 1958, in IAU Symp. 6, Electromagnetic Phenomena in Cosmical Plasma, ed. B. Lehnert (New York: Cambridge Univ. Press), 123
 Vainshtein, S. I., & Cattaneo, F. 1992, ApJ, 393, 165
 Vishniac, E. T. 1995a, ApJ, 446, 724
 ———. 1995b, ApJ, 451, 816